Am J Physiol Renal Physiol 305: F1574–F1584, 2013.
First published October 2, 2013; doi:10.1152/ajprenal.00382.2013.

A test of the hypothesis that oxalate secretion produces proximal tubule crystallization in primary hyperoxaluria type I

Elaine M. Worcester,[1] Andrew P. Evan,[2] Fredric L. Coe,[1] James E. Lingeman,[3] Amy Krambeck,[4] Andre Sommers,[5] Carrie L. Phillips,[6] and Dawn Milliner[7]

[1]*Nephrology Section, University of Chicago, Chicago, Illinois;* [2]*Department of Anatomy and Cell Biology, Indiana University School of Medicine, Indianapolis, Indiana;* [3]*Department of Urology Indiana University School of Medicine, Indianapolis, Indiana;* [4]*Department of Urology, Mayo Clinic, Rochester, Minnesota;* [5]*Department of Chemistry and Biochemistry, Miami University, Oxford, Ohio;* [6]*Department of Pathology, Indiana University Health, Indianapolis, Indiana; and* [7]*Division of Nephrology, Departments of Internal Medicine and Pediatrics, Mayo Clinic, Rochester, Minnesota*

Submitted 3 July 2013; accepted in final form 30 September 2013

Worcester EM, Evan AP, Coe FL, Lingeman JE, Krambeck A, Sommers A, Phillips CL, Milliner D. A test of the hypothesis that oxalate secretion produces proximal tubule crystallization in primary hyperoxaluria type I. *Am J Physiol Renal Physiol* 305: F1574–F1584, 2013. First published October 2, 2013; doi:10.1152/ajprenal.00382.2013.—The sequence of events by which primary hyperoxaluria type 1 (PH1) causes renal failure is unclear. We hypothesize that proximal tubule (PT) is vulnerable because oxalate secretion raises calcium oxalate (CaOx) supersaturation (SS) there, leading to crystal formation and cellular injury. We studied cortical and papillary biopsies from two PH1 patients with preserved renal function, and seven native kidneys removed from four patients at the time of transplant, after short-term (2) or longer term (2) dialysis. In these patients, and another five PH1 patients without renal failure, we calculated oxalate secretion, and estimated PT CaOx SS. Plasma oxalate was elevated in all PH1 patients and inverse to creatinine clearance. Renal secretion of oxalate was present in all PH1 but rare in controls. PT CaOx SS was >1 in all nonpyridoxine-responsive PH1 before transplant and most marked in patients who developed end stage renal disease (ESRD). PT from PH1 with preserved renal function had birefringent crystals, confirming the presence of CaOx SS, but had no evidence of cortical inflammation or scarring by histopathology or hyaluronan staining. PH1 with short ESRD showed CaOx deposition and hyaluronan staining particularly at the corticomedullary junction in distal PT while cortical collecting ducts were spared. Longer ESRD showed widespread cortical CaOx, and in both groups papillary tissue had marked intratubular CaOx deposits and fibrosis. CaOx SS in PT causes CaOx crystal formation, and CaOx deposition in distal PT appears to be associated with ESRD. Minimizing PT CaOx SS may be important for preserving renal function in PH1.

primary hyperoxaluria; calcium oxalate; renal histopathology; proximal tubule

AMPLE EVIDENCE SUGGESTS THAT calcium oxalate (CaOx) crystals may injure proximal tubule (PT) cells (8, 43, 52) and could potentially lead to cortical injury and renal failure in animals (28–29) and humans (9, 24). However, whether or not formation of CaOx crystals in the renal cortex is an initiating event in the renal damage seen in human primary hyperoxaluria type 1 (PH1) is unclear. Kidneys from PH1 patients with end stage renal disease (ESRD) contain more cortical CaOx crystals than are found in other ESRD patients (39), but this could reflect the higher plasma oxalate concentrations present in PH1 patients with renal failure (24): the abundant crystals could be secondary to renal failure in PH1. Alternatively, high oxalate production and excretion in PH1 may cause PT crystals as a primary event, possibly even when renal function is near normal. For example, oxalate loading of animals produces cortical CaOx crystallizations in PT, especially the S3 segment (30, 31), as an early event. Despite this body of data, the exact sequence of events that produce ESRD in humans with PH1 remains unclear.

To further the problem, we propose the hypothesis that high oxalate entry into PT from filtration and secretion creates PT CaOx supersaturation (SS) that leads to CaOx crystal formation, even when renal function is normal, causing kidney injury and renal failure. One test of our hypothesis is to determine if PT CaOx SS is plausible in PH1 patients. A second test is to ask if CaOx crystals can be demonstrated in PT of PH1 patients whose renal function is still near normal and whose cortical cells are undamaged. Finally, because water extraction is most complete in the S3 segment of the PT, we should be able to demonstrate preferential CaOx accumulation at that site.

To perform the three needed tests, we have studied seven kidneys from four PH1 patients with ESRD, as well as both papillary and cortical biopsies from two PH1 patients who had near normal renal function and were studied during percutaneous nephrolithotomy (PNL). One of the two was studied on two occasions. Two more PH1 patients underwent intraoperative imaging during PNL without biopsy, one of whom had pyridoxine-sensitive PH1. Blood and urine studies were available on all eight patients.

With the use of these eight patients, and three additional PH1 cases from whom we did not obtain renal tissue or intraoperative imaging but did obtain plasma and urine oxalate on multiple occasions, we have been able to perform all three tests of our hypothesis. Our observations during the course of this work also allow us to present the surgical anatomy and histopathology of early PH1, not hitherto described.

METHODS

Subjects

We have studied renal tissue and/or intraoperative images from eight patients, and blood and urine oxalate levels from these patients as well as three more patients from whom we did not obtain tissue or images. All 11 had genetically proven PH1, but there were no 2 patients with the same genotype. Kidneys from *patients 1*, *2*, *4*, and *5* (Table 1) were obtained by native nephrectomy at the time of renal transplantation. *Patients 6* and *7* underwent intraoperative imaging and papillary and cortical biopsy during PNL. *Patient 7* had ureter-

Address for reprint requests and other correspondence: E. M. Worcester, Nephrology Section, MC5100, Univ. of Chicago, School of Medicine, 5841 South Maryland Ave., Chicago, IL 60637 (e-mail: eworcest@uchicago.edu).

Table 1. *Clinical characteristics of patients who had surgery*

Pt	Sex	Age at First Stone, yr	Age at Dx of PH1, yr	Stones (#)	Stone Treatments: ESWL	Stone Treatments: URS	Stone Treatments: Surgery type (#)	Presenting Symptom	Age at ESRD, yr	Time on Dialysis, mo	Age at Time of Procedure, yr	Type of Procedure
1	M	37	47	>20	4	1	–	Stone	56	2	56	LKT, bilat native Nx
2	F	–	<1	–	–	–	–	Failure to thrive, CKD	<1	15	2	LKT, bilat native Nx
3	M	4	4	>10	–	3	PNL (4)	Stone	–	–	23	PNL
4	F	25	46	>20/>10	~10/1	–	L Nx/Tx Nx	Stone	43/46	24/19	48	LKT, native R Nx
5	M	2	3	>10	4	4	–	Stone	19	9	20	LKT, bilat native Nx
6	F	2	2	7	–	–	NL, PNL (1)	Stone	–	–	37	PNL, Bx
7	M	3	3	14	3	4	PNL (2)	Stone	24	–	21	URS
											23	PNL, Bx
11	M	15	24	>20	1	–	PNL (2) Open (4)	Stone	67	5	66	PNL

Pt, patient; M, male; F, female; Dx, diagnosis; PH1, primary hyperoxaluria type 1; ESWL, extracorporeal shock wave lithotripsy; URS, ureteroscopy; PNL, percutaneous nephrolithotomy; Nx, nephrectomy; Tx, transplant; NL, nephrolithotomy; CKD, chronic kidney disease; ESRD, end stage renal disease; LKT, liver and kidney transplant; Bx, papillary biopsy.

oscopy with mapping (no biopsy) and then a PNL procedure with biopsy 2 yr later; this permitted mapping twice. The patient subsequently went on to ESRD over the next 12 mo. *Patients 3* and *11* had only intraoperative imaging via PNL. *Patient 11* became dialysis dependent 38 days postprocedure (PNL). At the time of PNL renal function was well preserved in all four patients; creatinine clearance values ($ml \cdot min^{-1} \cdot 1.73\ M^{-2}$) were as follows: 93 ± 8, 74 ± 6, 123 ± 16, and 70 ± 7 for *patients 3*, *6*, *7*, and *11*, respectively. All eight patients with renal tissue and/or imaging, except *patient 2*, formed pure CaOx stones; *patient 2* was an infant who formed no stones (Table 1). *Patients 8-10* provided only blood and urine measurements. The work was Institutional Review Board approved at both Mayo Clinic (no. 11–001702, 11–005413, and 07–008751) and Indiana University (no. 98–073). Patients are numbered in order of accession.

Clinical Laboratory Studies

Twenty-four hour urine samples and corresponding blood samples were collected for clinical management at Mayo Clinic while patients were eating their free choice diet. Because patients contributed variable numbers of samples over time periods ranging from 1 to 19 yr (median = 5 and mean = 6.6), and encompassing periods pre- and posttransplant, the individual contributions of each patient to our plasma and urine samples (numbers and timing of samples) are documented in Table 2. A total of 98 measurements of plasma and/or urine oxalate were collected over the course of treatment, including periods before onset of ESRD and after kidney-liver transplant in 4 patients. Of the 98 measurements, 61 instances had plasma and urine oxalate and creatinine obtained at the same time, allowing calculation of oxalate secretion and 82 had urine oxalate measurement with serum and urine creatinine, allowing calculation of PT CaOx SS (Table 3). Each patient had at least one such measurement, although in two cases the necessary information was only available after transplant. Twenty-four-hour urines were collected for clinical management in *patient 3* before and during treatment with pyridoxine. Urine oxalate was greatly elevated in all cases (Table 3) except for the one pyridoxine-responsive patient. Laboratory methods are detailed in prior publications (13, 17, 36, 58).

Because children and adults are analyzed together, we have expressed creatinine clearance, urine oxalate excretion, and urine volume per 1.73 M^2 (Table 3). Values are means ± SE for creatinine clearances (in $ml \cdot min^{-1} \cdot 1.73\ M^{-2}$). In those patients who underwent renal transplant, data are reported separately for the pre- and post-transplant periods. In three patients who eventually developed ESRD (*patients 1*, *5*, and *7*), laboratory data spanned periods in which renal function changed markedly. In these patients, the median creatinine clearance (CCr) was determined for the available data, and laboratories reported separately for periods in which CCr was above (H) or at-or-below (L) the median value.

Biopsy Protocol and Plaque Area Determination

During PNL all accessible papillae in *patients 3*, *6*, *7*, and *11* were digitally imaged as described elsewhere for determination of plaque area (17, 32). Biopsies were taken from the upper pole, interpolar, and lower pole papillae and cortex in *patients 6* and *7*. Both kidneys from *patients 1* and *2* were studied via ex vivo ureteroscopy to mimic the intraoperative mapping studies.

Tissue Analysis

General. Eight papillary and four cortical biopsies from *patients 6* and *7*, along with papillary and cortical samples from all four nephrectomy cases, were studied using light microscopy. All specimens were immersed in 5% paraformaldehyde in 0.1 mol/l phosphate buffer pH 7.4 (PPB).

Light microscopy. Papillary and cortical specimens fixed in PPB were dehydrated through a series of graded ethanol concentrations to

Table 2. *Counts of serum and urine samples for oxalate SS and secretion by subject*

	Pt 1	*Pt 2*	*Pt 3*	*Pt 4*	*Pt 5*	*Pt 6*	*Pt 7*	*Pt 8*	*Pt 9*	*Pt 10*	*Pt 11*	*All*
Age span	48–57	1–3	4–22	47–49	13–20	37–9	5–24	4–9	13–19	57–59	66	
Pre-ESRD	10, 8, 8	2, 0, 0	15, 15, 11	3, 0, 0	11, 7, 1	4, 4, 1	13, 10, 5	11, 10, 9	15, 15, 14	4, 4, 4	2, 2, 2	90, 75, 55
Post-Tx	2, 2, 2	2, 1, 1		3, 3, 2	1,1,1							8, 7, 6
Total	12, 10, 10	4, 1, 1	15, 15, 11	6, 3, 2	12, 8, 2	4, 4, 1	13, 10, 5	11, 10, 9	15, 15, 14	4, 4, 4	2, 2, 2	98, 82, 61

Counts are total number of samples reporting *1*) either serum or urine oxalate, *2*) urine oxalate molarity with both serum and urine creatinine molarities (for calculation of proximal tubule supersaturation (SS), and *3*) serum and urine oxalate and creatinine molarities for calculation of oxalate secretion. Age spans are from first to last set of measurements (yr). Pre-ESRD, measurements obtained before end stage renal disease with dialysis; Post-Tx, measurements obtained after liver kidney transplant.

Table 3. *Selected laboratory values by subject*

Subject	Type	*N*	U OX, mmol/day	P OX, uM/l	CCR, ml/min	FL OX, umol/h	Ox Sec, umol/h	SSOX
1	N Pre Tx (H)	4	2.4 ± 0.3	9 ± 3	83 ± 4	44 ± 11	57 ± 6	3 ± 0.5
1	N Pre Tx (L)	6	2.0 ± 0.5	17 ± 7	52 ± 6	43 ± 12	41 ± 10	5 ± 2
1	N Post Tx	2	0.4 ± 0.02	2 ± 1	57 ± 3	6 ± 2	10 ± 1	0.7 ± 0.01
2	N Pre Tx	2	–	109 ± 25	–	–	–	–
2	N Post Tx	2	2.8	6 ± 2	33	16	99	8.7
3	PNL	15	0.7 ± 0.1	3 ± 1	93 ± 8	19 ± 4	6 ± 5	1.1 ± 0.4
4	N Pre Tx	3	–	107 ± 19	–	–	–	–
4	N Post Tx	3	1.6 ± 0.4	18 ± 1	33 ± 8	28 ± 10	26 ± 11	4.9 ± 0.04
5	N Pre Tx (H)	5	2.5 ± 0.5	7 ± 4	95 ± 4	38 ± 27	36 ± 26	2.8 ± 0.6
5	N Pre Tx (L)	3	2.3 ± 0.2	–	78 ± 6	–	–	3.1 ± 0.4
5	N Post Tx	1	0.5	1.9	93	11	10	0.5
6	PNL	4	1.8 ± 0.3	4	74 ± 6	20	42	2.7 ± 0.7
7	PNL (H)	5	2.1 ± 0.4	12 ± 1	159 ± 10	110 ± 24	−29 ± 32	1.4 ± 0.3
7	PNL (L)	5	1.6 ± 0.1	8 ± 2	88 ± 20	54 ± 23	11 ± 28	2.7 ± 0.8
8	No surg	10	2.5 ± 0.1	9 ± 2	38 ± 3	19 ± 4	88 ± 6	7.4 ± 0.8
9	No surg	15	1.7 ± 0.2	9 ± 1	59 ± 4	31 ± 4	40 ± 6	3.1 ± 0.2
10	No surg	4	3.1 ± 0.2	32 ± 12	57 ± 15	81 ± 15	48 ± 14	7 ± 2
11	PNL	2	1.6 ± 0.02	11 ± 2	70 ± 7	43 ± 5	23 ± 4	2.4 ± 0.3

Values are means ± SE; N, patient who underwent native nephrectomy; PNL, patient studied at time of PNL; No surg, patient contributing no surgical data; Pre Tx, pretransplant; Post Tx, posttransplant; H, values when CCR was above median value; L, values when CCR was below median value; *n*, number of measurements; U Ox, urine oxalate (normal <0.46 mmol/day); P Ox, plasma oxalate (normal <1.8 uM/l); CCR, creatinine clearance per 1.73 m^2; FL OX, filtered oxalate; Ox Sec, absolute oxalate secretion; SSOX, calculated proximal tubule CaOx supersaturation. Missing SE indicate <3 measurements for that variable.

100% ethanol before embedment in a 50/50 mixture of Paraplast Xtra (Fisher) and Peel-away Micro-Cut (Polysciences). Twelve serial sections from each specimen were cut at 4 μm and stained with the Yasue metal substitution method for calcium histochemistry (16). Hematoxalin and eosin for routine histological examination, Jones′ silver stain for the semiquantitation of glomerulosclerosis, and the Masson Trichrome stain to determine sites of interstitial fibrosis at the light microscopic level (Table 4). An additional set of serial sections was cut at 7 μm for infrared analysis. Because of the large amount of mineral in some of the kidney samples and the high degree of tissue injury, we used conjugated peanut agglutinin lectin (*Arachis hypogaea*) to specifically stain distal tubules and lotus lectin (*Lotus tetragonolobus*) for proximal tubules (23, 51). Medullary collecting ducts were easily identified by their branching patterns while the peanut agglutinin and lotus lectins permitted identification of cortical collecting ducts by exclusion. Tissues were viewed using fluorescence microscopy to visualize lectin staining.

In a double blind design, a renal pathologist (C. Phillips) performed a semiquantitative analysis (18) using the Jones' silver stained or periodic acid Schiff-stained cortical sections from all patients from whom tissue was available. Tubular atrophy and interstitial fibrosis were independently scored on a scale of 0 to 3 (0 = none, 1 = mild or <34% of sample, 2 = moderate or 34–66%, and 3 = severe or >66%). Glomerulosclerosis was defined as increased mesangial matrix with or without wrinkling, thickening, and/or collapse of glomerular basement membranes. Sclerosis of individual glomeruli was scored as segmental (<25% = mild, 25–75% = moderate), or global (>75% = severe or total obsolescence). The total number of glomeruli observed and the number of glomeruli in each of the three categories of sclerosis were recorded.

Hyaluronan staining. Hyaluronan was localized using biotinylated hyaluronan acid binding protein, in both routine formalin fixed tissue and the 10% formalin in 70% ethanol and 5% glacial acetic acid biopsies of the cortex and papilla from *patients 1*, *2*, *4*, *5*, *6*, and *7*. Paraffin-sectioned tissue (cut at 4 μm) was mounted on glass slides and processed as described in our previous publication (11). Controls were performed with the elimination of the primary antibody and showed no staining.

Crystal deposits. INFRARED. Attenuated Total Internal Reflection (ATR) Fourier Transform Infrared Microspectroscopy (μFTIR) was used as described elsewhere (16) to identify mineral types in crystal deposits.

MICROCOMPUTED TOMOGRAPHY. All papillary biopsies underwent microcomputed tomography (μCT) analysis with the SkyScan-1072 (Vluchtenburgstraat 3, B-2630 Aartselaar, Belgium) high-resolution desk-top μCT system allowing nondestructive mapping of the location and size of the crystalline deposits within a biopsy specimen. This μCT system can generate a tissue window so that both the mineral deposit and tissue organization are seen at the same time. For this protocol, biopsies are quickly dipped in a 1:10 dilution of Hypaque (50%; Nycomed, Princeton, NJ)/PBS and then coated with a thin layer of paraffin and mounted in the center of a small chuck that is then locked into place in the machine. The sample was positioned in the center of the beam, and the system configuration was set at 35 kV, 209 A, 180° rotation, with flatfield correction. Images were saved to CDs and reconstructed with Cone-Reconstruction software by SkyScan. These images were then reconstructed into 3D images with SkyScan's CTAn + CTVol software. These images allowed us to properly orient each biopsy for future light microscopic analysis. The 3D software was used to generate quantitative measurements of deposit size (mm) and density (mm^3).

Calculation of Oxalate Secretion and PT SS

Absolute oxalate secretion (Sox) is calculated by mass balance (*Eq. 1*):

$$\text{Sox} = (\text{Uox} \times \text{V}) - (\text{g} \times \text{Pox}) \quad (1)$$

where U and P are urine and plasma oxalate concentrations, g is GFR as estimated by creatinine clearance, V is urine flow rate in the same units as g ($ml \cdot min^{-1} \cdot 1.73\ M^{-2}$), and g × Pox is oxalate filtered load (oxalate is freely ultrafiltered; Ref. 60).

Inputs of oxalate into PT are filtration and secretion; urine oxalate is assumed to equal the sum of filtered and net secreted oxalate (secretion minus any subsequent PT reabsorption). A crucial assumption is that oxalate is neither added to or removed from tubule fluid beyond the PT S3 segment; this is probable since only the proximal tubule is known to contain both apical (SLC26a6) and basolateral (SLC26a1) oxalate transporters, as would be required for net secretion or absorption of oxalate from tubule fluid (1). The fluid available to dissolve the oxalate is g minus the fraction of g reabsorbed: g(1 − r) where r is the fraction of g reabsorbed. The term (1 − r) falls along the PT reaching a minimum in the last portion, S3:

$$\text{PTox} = (\text{V} \times \text{Uox})/\text{g}(1 - \text{r}) \quad (2)$$

where PTox is the molar concentration of oxalate in PT at the value of r achieved in the S3 segment, and Uox is urine oxalate molarity;

units of PT and urine oxalate concentration will match; V is urine flow rate, and g is GFR both in the same units.

Equation 2 reduces to *Eq. 3* given that $g = V \times (Ucr/Pcr)$:

$$PTox = \left[Uox/\left(U/P\right)cr\right] \times \left[1/\left(1 - r\right)\right] \quad (3)$$

Essentially *Eq. 3* performs *2* separate transformations. Dividing urine oxalate molarity by the urine to plasma creatinine concentration ratio removed effects of all water extraction along the entire nephron. The term [1/(1 − r)] adds back effects of water removal along the PT.

Values for r, estimated in normal humans from lithium clearances, range from 75 to 90% (2, 4, 19, 54). In patients with chronic kidney disease (creatinine values ~3.5 mg/dl), r averaged 75% (10, 44, 50). Because loop and distal reabsorption of lithium cannot be ruled out or quantified in humans, r may be less than these estimates. In animals, micropuncture measurements of PT water reabsorption using tubule fluid to plasma inulin ratios range from 44 to 67%, but these measurements may not include all of the cortical convolution and neglect reabsorption in the S3 segment (9, 31, 44). Given these observations we have chosen 75% reabsorption, which creates a fourfold increase in PT oxalate from water extraction: in other words 1/1 − r = 4.

If Uox is in $M \times 10^{-6}$ and ultrafiltrate (UF) calcium (UFca) is $M \times 10^{-3}$, which are customary, the PT molar concentration product is in $M^2 \times 10^{-9}$. We (55) have found an average value of 40×10^{-9} M^2 for this concentration product in human plasma ultrafiltrates incubated at 37°C with CaOx seed crystals for an interval long enough to achieve equilibrium. Therefore, PT SS, the ratio of the molar product in PT to that at equilibrium, is calculated as:

$$PTss = \left[UFca \times PTox\right]/40 \quad (4)$$

An SS value of 1 is by definition the empirical solubility since the denominator was measured in ultrafiltrates in equilibrium with CaOx crystals. Values <1 imply crystals will dissolve; values >1 indicate a driving force for crystal formation.

Statistical Methods and Analysis

Means ± SE were calculated for the key variables of interest: plasma oxalate molarity, urine oxalate excretion, urine volume flow rate, CCr, oxalate filtered load, and SS. Linear regression was used to assess relationships among plasma oxalate and CCr, urine oxalate excretion, and both filtered loads of oxalate and SS. Calculations were performed using conventional software (Systat, Point Richmond, CA).

RESULTS

Patients

We obtained data from 11 patients; clinical data are shown for all patients who had a surgery (Table 1). Three further PH1 patients who did not have surgery or ESRD contributed plasma and urine oxalate measurements. The number and timing of samples from each patient is shown in Table 2. Routine laboratory values from all 11 patients documented hyperoxaluria (Table 3). All cases were verified as PH1 by genetic analysis.

Three Hypothesis Tests

Plasma and urine oxalate, oxalate secretion, and PT CaOx SS. Plasma oxalate concentration and creatinine clearance were inversely associated (Fig. 1, *top left*). Urine oxalate excretion increased in parallel with oxalate filtered load (Fig. 1, *top right*) and most points lie above the diagonal line of identity indicating oxalate secretion. The cluster of points from our prior studies (4) of normal subjects and idiopathic calcium stone formers (Fig. 1, *top right*, grey circles) does not depart from the line of identity indicating that secretion is of minor overall quantitative significance in these subjects. Absolute oxalate secretion rates for PH1 patients almost all exceeded zero (Fig. 1, *bottom left*). Values from the ESRD cases obtained before the onset of dialysis (black circles), and the three PH1 patients for whom we did not have tissue (grey triangles), far exceeded values of the PNL cases (black triangles). Posttransplant secretion values (grey diamonds) were similar to those of PNL patients. Our prior study patients, being normal subjects and idiopathic calcium stone formers, showed the expected secretion values that varied from modestly below to modestly above zero (grey circles).

Proximal tubule fluid CaOx SS (Fig. 1, *bottom right*) exceeded 1 (horizontal line) in a majority of the PH1 patients whereas values in our prior normals and calcium stone formers were all <1, as were three of the posttransplant values and the PH1 patient who was pyridoxine responsive (Table 3). PT SS and urine oxalate excretion were directly correlated. It tended to fall after transplant as urine oxalate fell. Overall, PT CaOx SS is plausible in a majority of PH1 patients but not in normal subjects.

Evidence for PT CaOx crystals in otherwise normal renal cortex of PH1 patients. The only cortical abnormality in our PNL cases was the presence of tiny birefringent crystals on the surfaces of a few PT cells identified via lectin staining as well as morphology (Fig. 2, *A* and *B*). These birefringent crystals were present in two PT of each patient. Being in outer cortex these must be S1 or S2 PT. Mean predicted PT SS values for the S3 segments of these two patients were about twofold (Table 3, *patients 6* and *7*). In other words, we found crystals in PT segments whose SS values would presumably be less than those of the S3 segment; finding the crystals proves that SS CaOx must exceed 1. The PT that had crystals at their brush borders (Fig. 2*B*) were otherwise normal appearing: no inflammation or fibrosis was found. Hyaluronan staining was negative (Fig. 2*C*). Masson trichrome staining showed no evidence of cortical interstitial fibrosis (Fig. 2*A*, *inset*).

Evidence for preferential deposition of CaOx crystals in S3 segments. In kidneys harvested shortly after onset of dialysis (Table 1, *patients 1* and *5*) tubule deposits concentrated at the corticomedullary junction within PT lumens, cells, and the surrounding interstitial space (Fig. 2, *D* and *E*). In other words, the crystals concentrated in the S3 segments. By contrast, in kidneys harvested after prolonged dialysis (Table 1, *patients 2* and *4*) widely scattered intraluminal deposits were found throughout the entire cortex (not shown). Crystals were identified as CaOx by birefringence and μFTIR.

All sites of intraluminal deposits, including both crystals and lining cells across the entire cortex of *patients 1*, *2*, *4*, and *5*, stained with hyaluronan (Fig. 2*F*, arrow). Hyaluronan staining also occurred in numerous normal appearing PT segments that contained no crystals (Fig. 2*F*, arrowheads). In the early ESRD cases, cortical and outer medullary collecting ducts contained few crystals and were negative for hyaluronan whereas PT in the same compartments contained masses of crystals (Fig. 2*E*) and were hyaluronan positive.

Additional Observations

During the course of our hypothesis testing we necessarily made additional observations that have not as yet been described: papillary vs. cortical disease in PH1 patients with well- preserved renal function studied via PNL biopsies, early vs. late ESRD

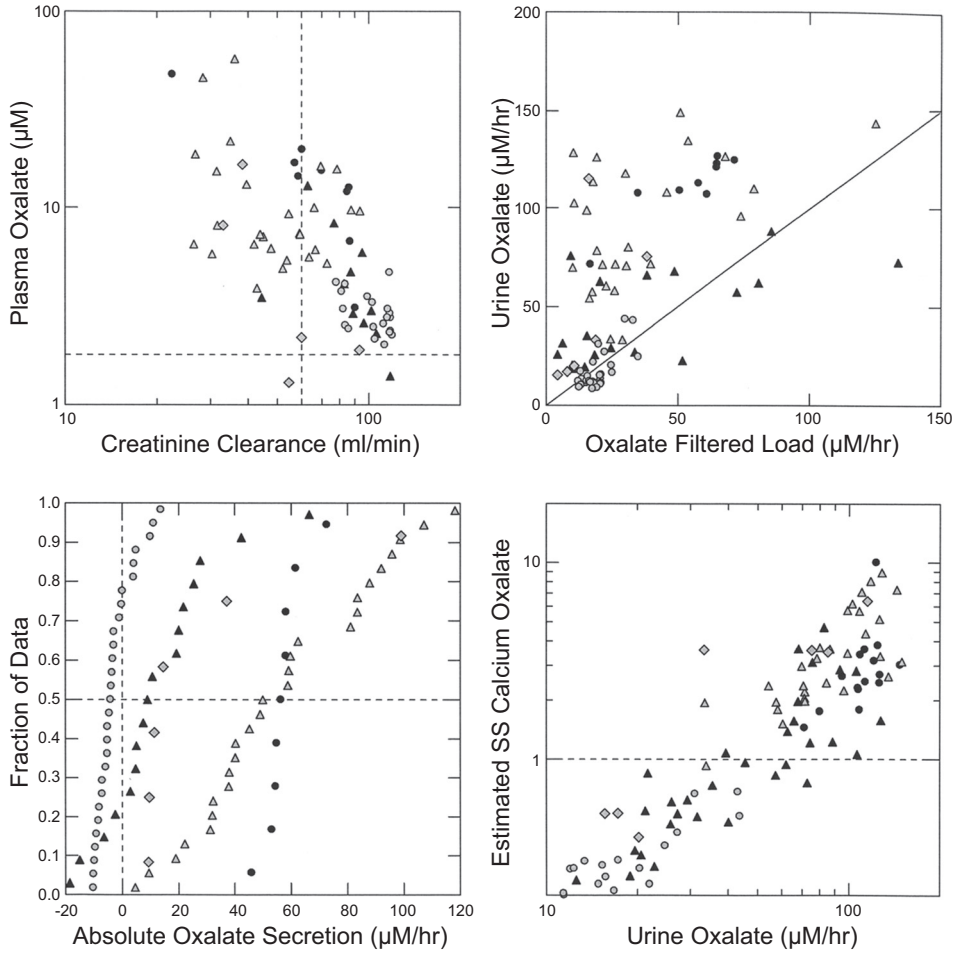

Fig. 1. Oxalate physiology and tubule calcium oxalate supersaturation. Plasma oxalate rises progressively with falling creatinine clearance (*top left*). Urine oxalate excretion rises with oxalate filtered load; a majority of points from primary hyperoxaluria type 1 (PH1) cases lie above the diagonal line of identity indicating that oxalate secretion is present (*top right*). Absolute oxalate secretion (*bottom left*) is minimal in ordinary stone formers (grey circles), but present to a varying extent in the PH1 patients. Estimated maximal proximal tubule CAOx supersaturation (see METHODS) rises with urine oxalate excretion (*bottom right*) and exceeds 1, the solubility limit, in a majority of PH1 patients. Symbols: black circles, *patients 1*, *2*, *4*, and *5* before transplant; black triangles, *patients 3*, *6*, *7*, and *11*; grey triangles, *patients 8*, *9*, and *10*; grey diamonds, PH1 *patients 1*, *2*, *4*, and *5* posttransplant; grey circles, idiopathic calcium stone formers and normals.

tissue changes in both papilla and cortex, and surgical anatomy of PH1 as viewed during intraoperative digital photography.

Relationship between papillary and cortical disease. PNL PAPILLAE. As in most stone diseases, papillary injury far exceeded cortical injury. Scattered inner medullary collecting ducts (IMCD) were plugged with CaOx crystals (Fig. 3*A*) which were birefringent (Fig. 3*A*, *top left inset*). Extensive interstitial fibrosis involved most of the papillary tip adjacent to and distant from plugged ducts (Fig. 3, *A–C*, arrowheads). Crystals were occasionally seen in IMCD cells but not the interstitium (Fig. 3*C*, arrows). In both patients IMCD plugs and cells were hyaluronan positive (Fig. 3*D*), as were some IMCD with no plugs and otherwise normal histology.

ESRD papillae and cortex. Papillary changes in ESRD kidneys (Fig. 4, *A* and *B*) are more severe than those of PNL cases, and cortical disease is massive. The density of IMCD plugging as seen on μCT (Table 4 and Fig. 4, *A* and *B*) was far greater than that observed in the PNL specimens (Fig. 3*A*, *bottom right inset*), and hyaluronan staining matched areas of fibrosis (Fig. 4*C*). In the cortex, tubular atrophy, interstitial fibrosis, and basement membrane thickening are extreme in all nephrectomy specimens (Table 4). Some regions (Fig. 4*D*) exhibit exotubulosis (55).

Endoscopic surgical anatomy. The papillary appearance of PH1 is so particular as to suggest the diagnosis during surgery, and we include it here as a clinical point that has not been described before. Randall's plaque was virtually absent in ESRD and PNL kidneys. Three of the five visualized papillae of *patient 3* were flattened and contained widely dilated Bellini ducts (BD) and yellow suburothelial deposits (Fig. 5*A*) known to reflect IMCD crystals (11, 12, 14, 17). The six visualized papillae of *patient 6* appeared normal except for scattered yellow deposits (Fig. 5*B*). *Patient 7* was studied twice. During the first procedure, 9 of 10 papillae were normal, 1 was flattened and had scattered yellow deposits (Fig. 5*C*), and a few dilated BD had protruding plugs. At the second procedure 2 yr later, a prior normal papillum had an eroded tip and a protruding plug with an overgrowing stone, meaning that damage had progressed (Fig. 5*D*). Ten months after the second procedure (Table 1), this patient had progressed to ESRD. The single papilla visualized in *patient 11* was normal (not shown). Papillary abnormalities were much more marked in the ESRD vs. the PNL cases (Fig. 5, *E* and *F*).

DISCUSSION

Tests of Our Hypothesis

Overview of the evidence supporting PT CaOx SS and PT CaOx crystal formation. Our measurements of urine oxalate along with calculations derived from mass balance indicate that PT tubule fluid is likely to be supersaturated with respect to CaOx in many patients with PH1. This calculation predicts that CaOx crystals might be found in the PT of patients with normal or near normal renal function, and we confirmed that prediction. In two of two PH1 PNL cortical biopsies we found birefringent crystals on the apical surfaces of PT cells that are

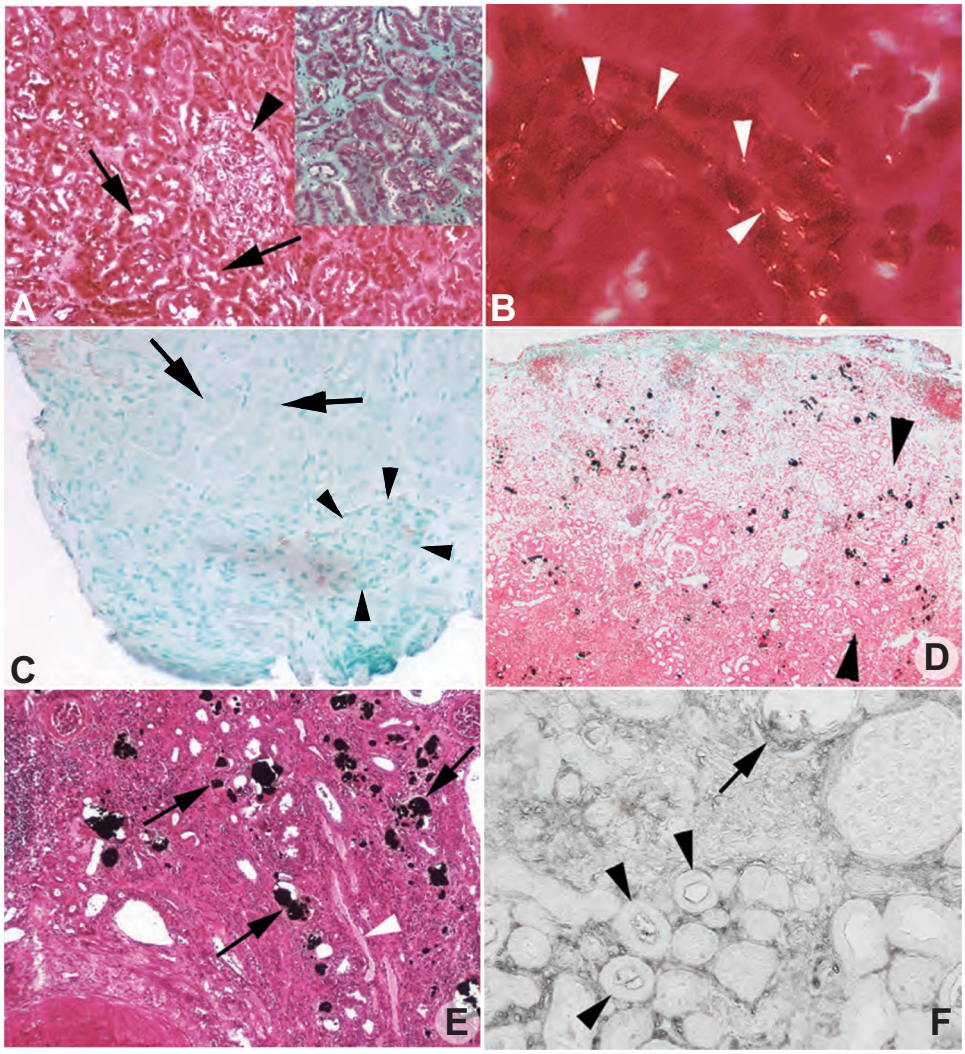

Fig. 2. Histopathologic images of cortical biopsies from percutaneous nephrolithotomy (PNL) and end stage renal disease (ESRD) PH1 patients. Yasue-stained cortical biopsy sections from PNL *patients 7* (creatinine clearance 123 ± 16; *A*) and *6* (creatinine clearance 74 ± 6) (not shown) revealed normal glomerular (arrowhead) and proximal tubule (arrows) morphology and no mineral deposits. Only minimal interstitial fibrosis was detected by Masson trichrome stain (*A*, *inset*) in the cortical biopsies. However, occasional small birefringent crystals (*B*, white arrows) were noted at the brush border of otherwise normal appearing proximal tubular cells of both PNL patients. No hyaluronan stained proximal tubular cells (arrows) or glomeruli (arrowheads) were seen in the cortical biopsies of *patients 6* (*C*) and *7* (not shown). Low magnification, light microscopy (*D*) shows widely scattered mineral deposition concentrated within the lumens of proximal tubular segments and the interstitium at the corticomedullary junction (between arrowheads, dark black-brown material) of ESRD *patient 1*. This crystalline pattern of the ESRD patient is in stark contrast to the lack of large cortical deposits in the PNL PH1 patients (*A*). *E*: Yasue-positive deposits in the lumen of the S3 segment of the proximal tubule shown here within the outer stripe of the outer medulla. A nearby outer medullary collecting duct is marked by a white arrowhead. Hyaluronan staining of cortical tissue from *patient 1* (*F*) shows intraluminal deposits (arrow) along with the apical cell surface of the adjacent proximal tubular cells positive for hyaluronan as well as positive staining of numerous nearby tubular segments (arrowheads), primarily proximal tubules, that do not possess intraluminal deposits. Original magnification: ×100 (*A* and *E*); ×200 (*B*); ×50 (*C*); ×75 (*D*); ×125 (*F*).

otherwise normal by appearance and by the absence of hyaluronan staining. The S3 segment is predicted to have the highest CaOx SS, and our studies of kidneys from patients who have not been on dialysis for an extended period support this prediction in showing that the corticomedullary PT are indeed a favored site of CaOx crystal accumulation. These observations and calculations converge on the idea that in PH1 CaOx SS in the S3 segment leads to CaOx crystallization. That we found crystals in the S1 or S2 segments in the PNL cases indicates that SS>1 must occur in segments even proximal to the S3 segment.

Uniqueness of the PT crystals. Such crystals have not been found in PT from any other human kidney stone disease phenotypes thus far and are therefore unlikely to be artifacts. Using oil immersion optics with polarization we found no crystals in either the cortex or the medulla from 30 idiopathic CaOx stone formers (11). We have found a few nonbirefringent crystals in the distal nephron segments but no crystals in the PT of patients with primary hyperparathyroidism (14) and cystinuria (12). Likewise, in none of the cortical sections of patients with brushite stones (17), small bowel disease (18), ileostomy (13), renal tubular acidosis (15), and obesity bypass (16) have we observed a single PT crystal. Put another way we have never encountered PT crystals in any stone forming state thus far apart from PH1. We emphasize this point so as to highlight the significance of the few tiny crystals we found in the PT of our two PNL patients.

Structure of the PT crystals. That the tiny crystals are CaOx is inferred but unproven. Birefringence is not a property of hydroxyapatite or brushite crystals. While monosodium urate and cystine crystals are strongly birefringent under the appropriate fixation methods, it is most unlikely that monosodium urate or cystine are forming in PT of PH1 patients (45).

Corticomedullary crystal accumulation. That the corticomedullary junction seems a preferred site for crystal formation, specifically in the S3 PT segments, is not incompatible with what is known about the physiology of this segment. The S3 segments lose water into the outer medullary interstitium that is rendered hypertonic to blood via NaCl reabsorption in water impermeable thick ascending limbs (25). Therefore, S3 segment tubule fluid would be predicted to have higher SS than the cortical PT segments and be a preferred site for crystals. Possibly, CaOx accumulation is also fostered by the abrupt reduction of tubule diameter at the transition from S3 to the thin descending limb of Henle's loop (26). Our PNL biopsies do not include S3 segments, so we cannot comment on crystal

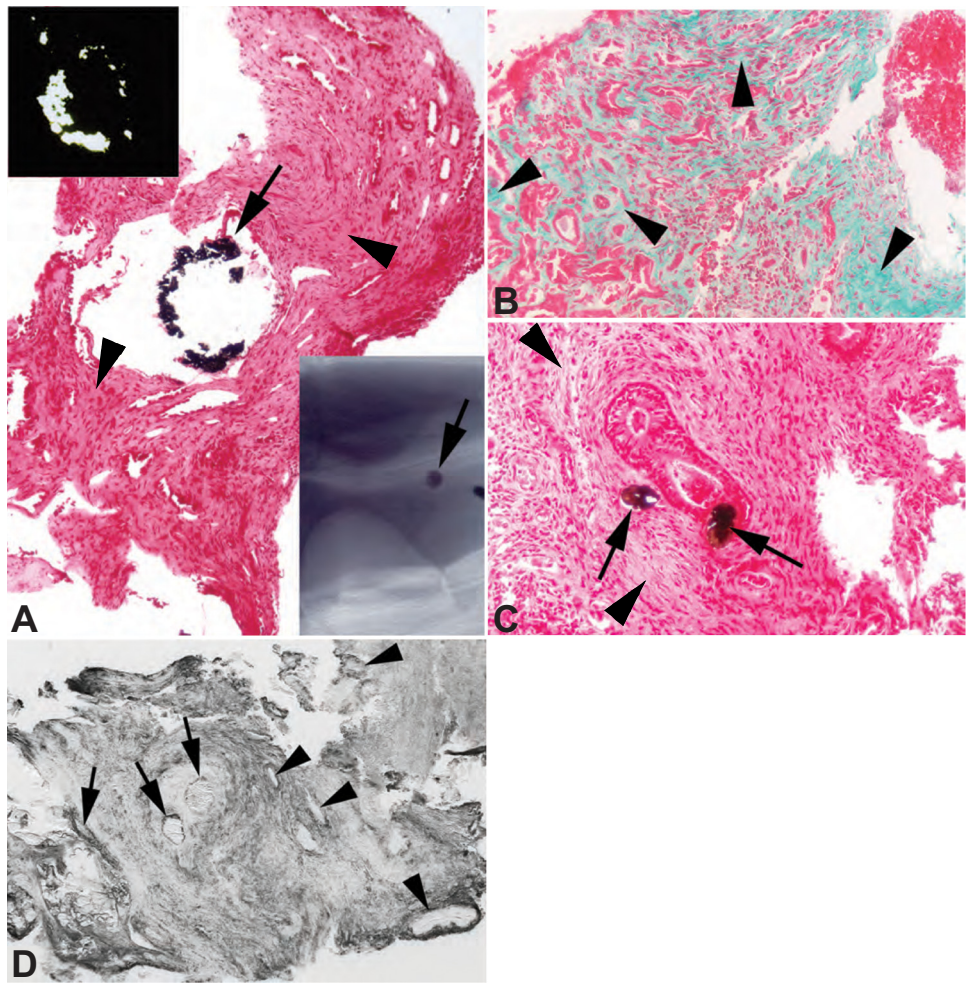

Fig. 3. Histopathologic changes of papillary biopsies from PNL PH1 patients. Yasue (*A* and *C*, arrows) and microcomputed tomography (μCT) images (*A*, *bottom right inset*) of papillary biopsies of both *patients 6* (creatinine clearance 74 ± 6) and *7* (creatinine clearance 123 ± 16) detected varying sized intraluminal deposits in a few inner medullary collecting ducts (IMCD). All deposits are birefringent (*A*, *top left inset*) when viewed by polarizing optics. Tissue sections stained with Masson trichrome to mark sites of fibrosis a greenish-blue revealed extensive interstitial fibrosis at sites adjacent to and away from (*B*, arrowheads) intraluminal deposits. Extensive interstitial fibrosis is also seen the Yasue-stained sections (*A* and *C*) at (arrows) and away from sites of deposits (arrowheads). Prominent hyaluronan staining was noted in biopsies from the papillary tip from both *patients 6* and *7* (*D*, *patient 6*). Two large intraluminal deposits (marked by arrows) show hyaluronan staining of the crystalline material as well as adjacent lining cells. A number of nearby IMCD segments with no intraluminal deposits also show hyaluronan staining of their apical cell surface (arrowheads). This staining pattern is in stark contrast to the lack of hyaluronan staining in the outer cortex of *patients 6* and *7*. Original magnification: ×75 (*A*); ×100 (*B* and *D*); ×200 (*C*).

formation there. Our evidence for preferential S3 crystal accumulation in ESRD kidneys seems convincing and is consistent with the physiology of that segment.

Potential Limitations of Our SS Calculation

Lithium estimates of reabsorption. To convert our estimates of PT fluid oxalate concentration into estimates of PT SS, we have used conventional means. In humans, endogenous lithium clearance is widely accepted as a marker for PT reabsorption, and most measurements give an average value of 80–90% of filtered fluid reabsorbed (6, 49). Possibly these high values could reflect lithium reabsorption beyond the PT in the loops of Henle or distal convolution (6, 49, 53, 57). To allow for this we have assumed reabsorption of 75%; this would increase tubule fluid oxalate concentration by fourfold (see METHODS). In essence by dividing urine oxalate molarity by the urine to plasma creatinine ratio (see METHODS, *Eq. 4*), we have removed all effects of water extraction along the nephron and have added back a fourfold concentration by water extraction in PT as estimated from lithium clearance. An unstated assumption is that all oxalate that enters PT, by filtration or net secretion, is excreted in the urine.

Effects of reduced GFR on PT reabsorption. One might guess that given chronic kidney disease PT fluid reabsorption would fall, but in animal micropuncture experiments fractional reabsorption of sodium and fluid is generally constant or falls only to a slight extent (22, 42, 61). In studies of humans with stages 2–4 nonnephrotic chronic kidney disease, lithium reabsorption has averaged 70–75%, close to our assumed value (10, 48); this means our calculations may well be valid even in PH1 patients who have lost significant renal function.

If a lower value for PT reabsorption is chosen, for example, 50%, the estimate for PT supersaturation would be about half as high. However, this would not affect our finding of crystals in PT on the biopsies of the patients who underwent biopsy at a time when renal function was still near normal or only modestly impaired. This would tend to strengthen the argument that PT is particularly vulnerable to crystal formation, even at relatively low levels of supersaturation, perhaps due to lack of crystallization inhibitors at this site in the nephron.

SS calculations. Throughout its length, PT fluid calcium concentration appears to approximate that of ultrafiltrate or ~1.1 mM/l (34). From this and estimated PT oxalate molarity we have calculated the CaOx molar product and divided by the empirical molar product in normal human plasma ultrafiltrate at equilibrium with CaOx crystals to obtain a relative SS; this is standard practice in kidney stone evaluation (19) and has been applied to estimate serum SS from oxalate retention in chronic kidney disease and dialysis (60). In perfused rabbit S3 segments Rouse et al. (41) observed what appeared to be active calcium reabsorption, so

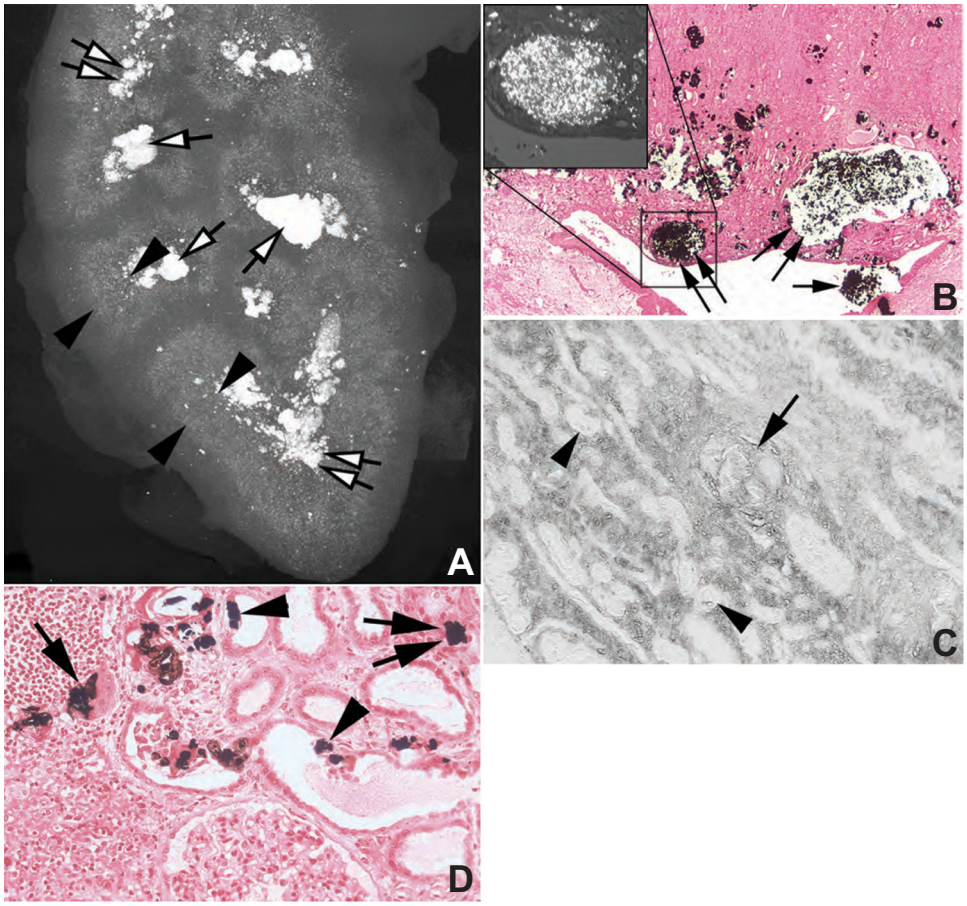

Fig. 4. Histopathologic changes in cortical and papillary biopsies from ESRD PH1 patients. *A*: μCT image of a kidney from *patient 1* that shows the pattern of crystalline deposits from the renal capsule to the papillary tip. While a few mineral deposits are present in the outer cortex (also see Fig. 2*D*), the majority of crystals are concentrated at the corticomedullary junction (between arrowheads) with extensive mineral deposition in the papillary tips (double white arrows) and stones in minor calyces (single white arrows). Light microscopy (*B*) shows large dilated IMCD filled with mineral (double arrows) and when examined by polarizing optics (*top left inset*) contains only birefringent material. Stone material (single arrow) was noted in the minor calyx. This pattern of mineral deposition is identical to that seen by μCT (Fig. 4*A*). The same pattern of hyaluronan staining seen in the cortex of *patient 1* (Fig. 2*F*) is noted in the inner medulla (*C*), hyaluronan positive intraluminal deposits (arrow) as well as staining of nearby nephron segments, in this case IMCDs (arrowheads) that do not possess intraluminal deposits. High magnification light microscopic images of the cortex shows crystalline deposits in the lumens (arrows) and cells (arrowheads) of primarily proximal tubules (*D*) as well as the interstitium (double arrows). Sites of exotubulosis (arrowheads) are noted in some proximal tubules. Extensive interstitial fibrosis encapsulates many cortical nephron segments (*D*). Original magnification: ×5 (*A*); ×50 (*B*); ×100 (*C*); ×125 (*D*).

possibly our assumption that PT calcium molarity equals that of plasma ultrafiltrates overestimates SS to some extent.

Links Among Secretion, Plasma Oxalate, PT SS, and Renal Function

Oxalate secretion. Proximal tubules are the known site of oxalate secretion presumably via SLC26a6 and a1 transporters (35, 46). Our measurements confirm oxalate secretion is the rule in PH1, whereas in normal subjects and common stone formers it is variable and of relatively trivial magnitude. Our PH1 patients have plasma oxalate concentrations 3 to 40 times above normal, which may be driving secretion but this cannot be rigorously tested in our experiments. In a general linear model with oxalate secretion as dependent and CCr, plasma oxalate, and urine oxalate as independents, secretion had large and expected partial correlations with CCr and urine oxalate excretion (−0.62 and 0.71, respectively, $P < 0.001$ for both) but not a significant one with plasma oxalate (0.051, $P = 0.7$). Since secretion is calculated as the difference between urine oxalate excretion and filtered oxalate load (the product of plasma oxalate and CCr), one cannot proceed further with stepwise regression because if either of the latter two is entered as a variable the other becomes required in a tautological fashion.

Effects of reduced GFR. Our calculation requires that CaOx SS in PT rise hyperbolically as GFR falls (see METHODS). Since the calculations are based on mass balance, and the obvious fact that oxalate production and excretion do not fall with falling GFR, we believe this is probably the fact and that, therefore, PT CaOx crystal formation is not rare in ordinary forms of chronic renal disease and certainly in the renal disease of PH1. This is beyond

Table 4. *Tissue, crystals, and pathology*

	Papillary Deposits		Cortical Pathology Score					
				Glomerular pathology				
Patient	Average size, mm	#/mm^3	#Glomeruli	Mild	Moderate	Global	Tubular atrophy	Interstitial fibrosis
1	1.9	27	11	1	7	3	3	3
2	1.2	27	19	1	2	16	3	3
4	1.8	25	22	0	0	22	3	3
5	1.5	29	18	1	17	0	3	3
6	0.3	2.4	5	5	0	0	1	1
7	0.6	3	2	2	0	0	1	1

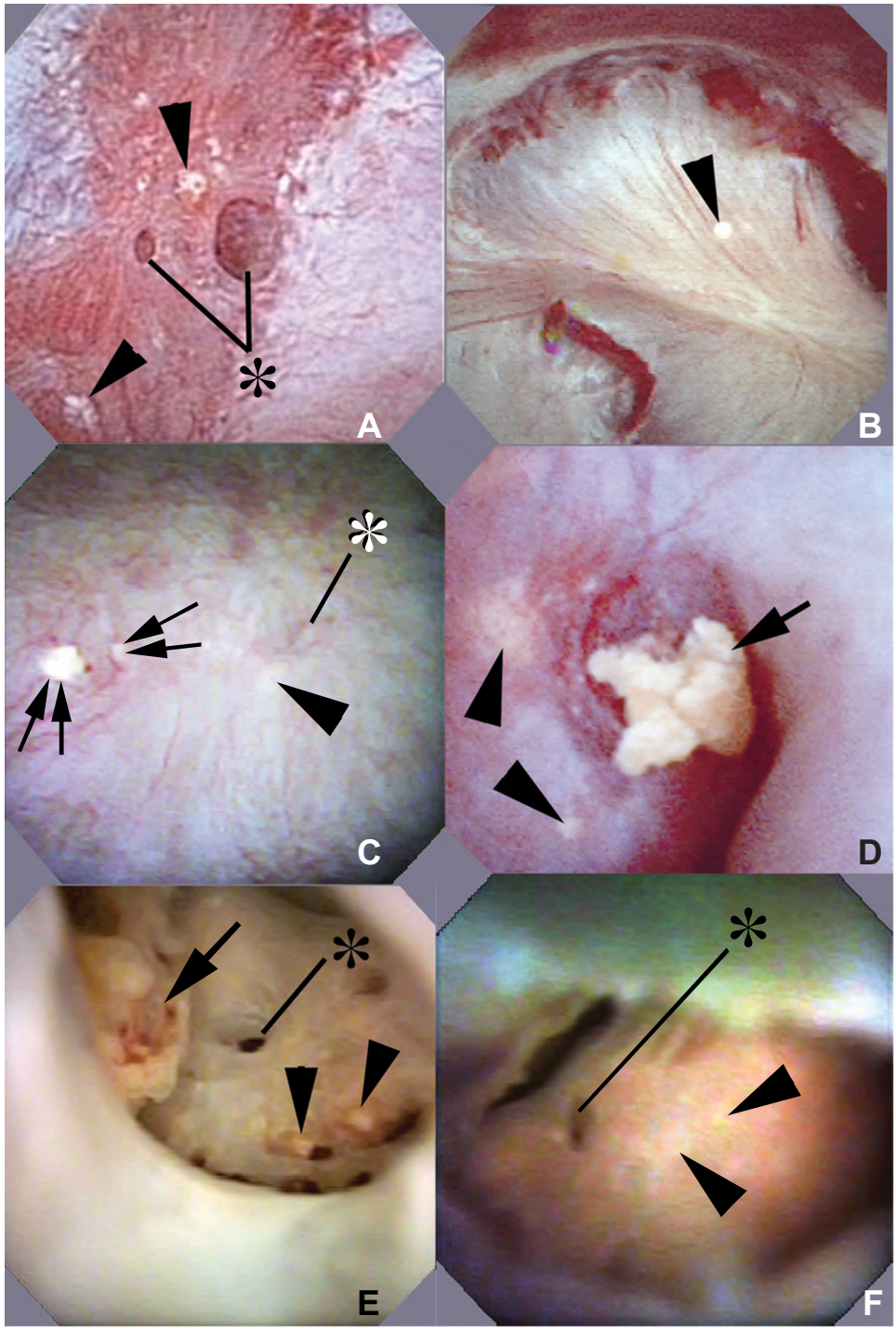

Fig. 5. Intraoperative and ex vivo endoscopic images of papillae from PNL (*cases 3*, *6*, and *7*) and ESRD (*cases 1* and *2*) PH1 patients. *A–D*: intraoperative endoscopic images collected at the time of mapping and stone removal from *patients 3* (*A*), *6* (*B*), and *7* (*C* and *D*). Papillary morphology varied from normal (*B* and *C*) to flattened (*A* and *D*). A few dilated ducts of Bellini (*A* and *C*, *) with (*C*, double arrows) and without (*A*, *) protruding plugs were seen scattered between sites of yellow plaque (arrowheads). The same kidney of *patient 7* seen in *C* was studied a second time 2 yr later and one papilla now showed an eroded tip and a protruding plug with a stone overgrowth not seen previously (*D*, arrow). With the use of ex vivo ureteroscopy, nonadherent stones (*E*, arrow) were noted lying on a papillary tip in *patient 1*, an adult with PH1 and ESRD. Removal of one of these stones revealed a dilated opening to a duct of Bellini (*E*, *). Small sites of yellow plaque (arrowheads) are noted nearby. *F*: ex vivo ureteroscopy image from *patient 2*, an infant with PH1 and ESRD. A dilated opening to a duct of Bellini (*) and sites of yellow plaque (arrowheads) appear similar to that seen in *patient 1* in *E*, however, no stones are found.

the scope of the present work but suggests that search for such crystals in renal biopsies might be productive.

Crystal Clearance Mechanisms and Crystal-Mediated Injury in PH1

Possible balance between crystal formation and clearance. The fact that PT SS seems common and persistent and that tiny crystals can be found in the absence of cell damage in PT suggests that some mechanisms must exist to clear crystals from the tubules so crystals do not accumulate. Indeed, PT cells can clear crystals via exotubulosis (55). We found this process in our ESRD kidneys and presume it can occur earlier in the disease. As well, some crystals can be taken up by PT cells, as we found in our ESRD samples, and digested in their lysosomes (34). The tiny crystals found in our PNL patients do not appear to have triggered inflammation, based on the absence of staining for hyaluronan (2, 55, 56). One might speculate that given SS as a driver of crystallization, and these cell processes, one can envision a kind of stable equilibrium between formation and removal that can be disturbed by in-

creases of PT fluid reabsorption, acute or chronic reductions of GFR both of which will increase PT CaOx SS, or a disturbance of clearance mechanisms.

Cortical injury. The links between CaOx crystals and PT cell damage have been described by others (8, 21, 27–31, 43, 52) and are beyond the scope of this report. Recently, two groups have reported that renal inflammation and tissue injury in rodent models of acute oxalate toxicity are mediated by NLRP3. The site of greatest injury in their studies was at the inner stripe of the outer medulla, as seen in the patients who had early ESRD (33, 38). Whether the tissue injury in PH1 is induced by the same mechanisms is unclear. Our work demonstrates that in patients with preserved renal function crystals form in PT without inducing tissue injury or inflammation demonstrable with standard histologic methods; what transforms this noninjurious crystal formation into the injury pattern seen in patients with early ESRD remains to be discovered. Quite possibly those patients with the highest PT SS may form the most PT crystals, trigger an inflammatory process leading to injury, and progress most rapidly to ESRD; this can be tested by prospective observational studies. Likewise episodic reductions in GFR may cause acute renal injury with rapid crystal deposition that eventuates in ESRD.

Papillary injury. Our PNL biopsies show that papillary injury far exceeds cortical injury in PH1 as it can in all kidney stone-forming phenotypes we have studied to date (12–18). We presume this disproportion of damage between papilla and cortex reflects the corresponding disproportion of CaOx SS and crystallization potential. Whereas cortical SS is predicted to be two- threefold (Table 3), urine SS for CaOx is always much higher (40). In idiopathic CaOx stone formers cortical SS is null, as shown in Fig. 1, and cortical tissue normal (not shown). In PH1 crystal deposition, although marked, is not greater than in such states such as renal tubular acidosis, but the amount of fibrosis is much greater. The mechanisms for this disproportion is presently unknown.

Clinical Implications

Possible importance of maintaining a high sodium intake. Factors that reduce GFR and/or increase PT reabsorption, such as extracellular volume depletion may well be dangerous in PH1. All stone patients have increased stone risks from dehydration (7); in PH1 not only papillary stones but PT crystals may be fostered. Water alone would not be predicted to have any effect on PT reabsorption since it would act by lowering vasopressin, which acts at later sites in the nephron; only high sodium intake can reduce PT reabsorption (47). Therefore, a high-salt diet might be of benefit, and sodium depletion from diet or diuretics might be harmful in PH1. Clinical trials would be needed to test these conjectures.

Surgical diagnosis. The unique surgical appearance of PH1 can alert clinicians to the diagnosis. Stones do not form on interstitial (Randall's) plaque but are either free in the collecting system or growing on plugs. IMCD plugging is common in calcium phosphate stone formers (15, 17), and those with hyperparathyroidism (14) and bowel diseases (13, 18), but PH1 patients form CaOx stones, and systemic diseases can be excluded clinically. In other words, a CaOx stone former with tubule plugging, minimal or no interstitial plaque, and no apparent systemic or bowel disease should raise suspicion of PH1 and be studied appropriately.

GRANTS

This work was supported by National Institute of Diabetes and Digestive and Kidney Diseases Grants PO1-DK-56788, DK-73354, U54-DK-083908 and the Oxalosis and Hyperoxaluria Foundation and funding from the National Center For Advancing Translational Sciences.

DISCLOSURES

No conflicts of interest, financial or otherwise, are declared by the author(s).

AUTHOR CONTRIBUTIONS

Author contributions: E.M.W., A.P.E., F.L.C., J.E.L., A.K., and D.M. conception and design of research; E.M.W., A.P.E., F.L.C., J.E.L., A.K., A.S., C.L.P., and D.M. performed experiments; E.M.W., A.P.E., F.L.C., J.E.L., A.K., A.S., C.L.P., and D.M. analyzed data; E.M.W., A.P.E., F.L.C., J.E.L., A.K., A.S., and D.M. interpreted results of experiments; E.M.W., A.P.E., F.L.C., J.E.L., A.S., and D.M. prepared figures; E.M.W., A.P.E., F.L.C., J.E.L., A.S., and D.M. drafted manuscript; E.M.W., A.P.E., F.L.C., J.E.L., A.K., C.L.P., and D.M. edited and revised manuscript; E.M.W., A.P.E., F.L.C., J.E.L., A.K., A.S., C.L.P., and D.M. approved final version of manuscript.

REFERENCES

1. **Alper SL, Sharma AK.** The SLC26 gene family of anion transporters and channels. *Mol Aspects Med* 34: 494–515, 2013.
2. **Asselman M, Verhulst A, van Bullegooijen ES, Bangma CH, Verkoelen CF, De Broe ME.** Hyaluronan is apically secreted and expressed by proliferating or regenerating renal tubular cells. *Kidney Int* 68: 71–83, 2005.
3. **Barbato A, Cappuccio FP, Folkerd EJ, Strazzullo P, Sampson B, Cook DG, Alberti KGMM.** Metabolic syndrome and renal sodium handling in three ethnic groups living in England. *Diabetologia* 47: 40–46, 2004.
4. **Bergsland KJ, Zisman AL, Asplin JR, Worcester EM, Coe FL.** Evidence of net tubule secretion in patients with calcium kidney stones. *Am J Physiol Renal Physiol* 300: F311–F318, 2011.
5. **Bochud M, Staessen JA, Maillard M, Mazeko MJ, Kuznetsova T, Woodiwiss A, Richart T, Norton G, Thijs L, Elston R, Burnier M.** Ethnic differences in proximal and distal tubular sodium reabsorption are heritable in black and white populations. *J Hypertens* 27: 606–612, 2009.
6. **Boer WH, Koomans HA, Dorhout Mees EJ.** Lithium clearance in healthy humans suggesting lithium reabsorption beyond the proximal tubule. *Kidney Int* 28: S39–S44, 1990.
7. **Borghi L, Meschi T, Amato F, Briganti A, Novarini A, Giannini A.** Urinary volume, water and recurrences in idiopathic calcium nephrolithiasis: a 5-year randomized prospective study. *J Urol* 155: 839–843, 1996.
8. **Byer K, Khan SR.** Citrate provides protection against oxalate and calcium oxalate crystal induced oxidative damage to renal epithelium. *J Urol* 173: 640, 2005.
9. **Cryer PE, Garber AJ, Hoffsten P, Lucas B, Wise L.** Renal failure after small intestinal bypass for obesity. *Arch Intern Med* 135: 1610–1612, 1975.
10. **Dhaun N, Ferro CJ, Davenport AP, Haynes WG, Goddard J, Webb DJ.** Haemodynamic and renal effects of endothelin receptor antagonism in patients with chronic kidney disease. *Nephrol Dial Transplant* 22: 3228–3234, 2007.
11. **Evan AP, Coe FL, Gillen D, Lingeman JE, Bledsoe S, Worcester EM.** Renal intraluminal crystals and hyaluronan staining occur in stone formers with bypass surgery but not with idiopathic calcium oxalate stones. *Anat Rec* 291: 325–334, 2008.
12. **Evan AP, Coe FL, Lingeman JE, Shao Y, Matlaga BR, Kim SC, Bledsoe SB, Sommer AJ, Grynpas M, Worchester EM.** Renal crystal deposits and histopathology in patients with cystine stones. *J Urol* 175: 498, 2006.
13. **Evan AP, Lingeman JE, Coe FL, Bledsoe SB, Sommer AJ, Williams JC Jr, Krambeck AE, Worcester EM.** Intra-tubular deposits, urine and stone composition are divergent in patients with ileostomy. *Kidney Int* 76: 1081–1088, 2009.
14. **Evan AE, Lingeman JE, Coe FL, Miller NL, Bledsoe SB, Sommer AJ, Williams JC, Shao Y, Worcester EM.** Histopathology and surgical anatomy of patients with primary hyperparathyroidism and calcium phosphate stones. *Kidney Int* 74: 223–229, 2008.

15. **Evan AP, Lingeman J, Coe F, Shao Y, Miller N, Matlaga B, Phillips C, Sommer A, Worcester E.** Renal histopathology of stone-forming patients with distal renal tubular acidosis. *Kidney Int* 71: 795–801, 2007.
16. **Evan AP, Lingeman JE, Coe FL, Parks JH, Bledsoe SB, Shao Y, Sommer AJ, Paterson RF, Kuo RL, Grynpas M.** Randall's plaque of patients with nephrolithiasis begins in basement membranes of thin loops of Henle. *J Clin Invest* 111: 607–616, 2003.
17. **Evan AP, Lingeman JE, Coe FL, Shao Y, Parks JH, Bledsoe SB, Phillips CL, Bonsib S, Worcester EM, Sommer AJ, Kim SC, Tinmouth WW, Grynpas M.** Crystal-associated nephropathy in patients with brushite nephrolithiasis. *Kidney Int* 67: 576–591, 2005.
18. **Evan AP, Lingeman JE, Worcester EM, Bledsoe SB, Sommer AJ, Williams JC Jr, Krambeck AE, Philips CL, Coe FL.** Renal histopathology and crystal deposits in patients with small bowel resection and calcium oxalate stone disease. *Kidney Int* 78: 310–317, 2010.
19. **Finlayson B.** Calcium stone: some physical and clinical aspects. In: *Calcium Metabolism in Renal Failure and Nephrolithiasis*, edited by David DS. New York: John Wiley & Sons, 1977, p. 337–382.
20. **Fliser D, Franek E, Joest M, Block S, Mutschler E, Ritz E.** Renal function in the elderly: impact of hypertension and cardic function. *Kidney Int* 51: 1196–1204, 1997.
21. **Hackett RL, Shevock PN.** Crystal-cell interaction: its role in the development of stone disease. In: *Calcium oxalate in Biological Systems*, edited by Khan, S. Boca Raton, FL: CRC, 1995.
22. **Hayslett JP.** Functional adaptation to reduction in renal mass. *Physiol Rev* 59: 137–163, 1979.
23. **Hennigar RA, Schulte BA, Spicer SS.** Heterogeneous distribution of glycoconjugates in human kidney tubules. *Anat Rec* 211: 376–390, 1985.
24. **Hoppe B, Kemper MJ, Bokenkamp A, Portale AA, Cohn RA, Langman CB.** Plasma calcium-oxalate supersaturation in children with primary hyperoxaluria and end stage renal disease. *Kidney Int* 56: 268–274, 1999.
25. **Jamison RL, Kriz W.** Thick ascending limb. In: *Urinary Concentrating Mechanism: Structure and Function*. New York: Oxford Univ. Press, p.173–188, 1985.
26. **Kaissling B, Kritz W.** Structural analysis of the rabbit kidney. *Adv Anat Embryol Cell Biol* 56: 1–123, 1979.
27. **Khan SR.** Crystal-induced inflammation of the kidneys: results from human studies animal models and tissue-culture studies. *Clin Exp Nephrol* 8: 75–88, 2004.
28. **Khan SR.** Reactive oxygen species as the molecular modulators of calcium oxalate kidney stone formation: Evidence from clinical and experimental investigations. *J Urol* 189: 803–811, 2013.
29. **Khan SR, Glenton PA, Byer KJ.** Modeling of hyperoxaluric calcium oxalate nephrolithiasis: experimental induction of hyperoxaluria by hydroxyl-L-proline. *Kidney Int* 70: 914–923, 2006.
30. **Khan SR, Hackett RL.** Calcium oxalate urolithiasis in rat: is it a model for human disease. *Scanning Microsc* 2: 759–774, 11985.
31. **Khan SR, Hackett RL.** Retention of calcium oxalate crystals in renal tubules. *Scanning Microsc* 5: 707–712, 1991.
32. **Kim SC, Coe F, Tinmouth WW, Kuo RL, Paterson RF, Parks JH, Munch LC, Evan AP, Lingeman JE.** Stone formation is proportional to papillary surface coverage by Randall's plaque. *J Urol* 173: 117–119, 2005.
33. **Knauf F, Asplin JR, Granja I, Schmidt IM, Moeckel GW, David RJ, Flavell RA, Aronson PS.** NALP3-mediated inflammation is a principal cause of progressive renal failure in oxalate nephropathy. *Kidney Int* 2013 Jun 5 [Epub ahead of print].
34. **Koomans HA, Boer WH, Dorhout Mees EJ.** Evaluation of lithium clearance as a marker of proximal tubule sodium handling. *Kidney Int* 38: 2–12, 1989.
35. **Kujala M, Tienari J, Lohi H, Elomaa O, Sariola H, Lehtnen E, Kere J.** SLC26A6 and SLC26A7 anion exchangers have a distinct distribution in human kidney. *Nephron Exp Nephrol* 101: e50–e58, 2005.
36. **Ladwig PM, Liedtke RR, Larson T, Lieske JC.** Sensitive spectrophotometric sssay for plasma oxalate. *Clin Chem* 51: 2377–2380, 2005.
37. **Lieski JC, Deganello S.** Nucleation, adhesion and internalization of calcium-containing urinary crystals by renal cells. *J Am Soc Nephrol* 14: S422–429, 1999.
38. **Mulay SR, Kulkarni OP, Rupanagudi KV, Migliorni A, Darisipudi MN, Vilaysane A, Muruve D, Shi Y, Munro F, Liapis H, Andres HJ.** Calcium oxalte crystals induce renal inflammation by NLRP3-mediated IL-1β secretion. *J Clin Invest* 123: 236–346, 2013.
39. **Murty MLN, Garg I, Date A, Jacob CK, Kirubakaran MG, Shastry JC.** Renal histology for the diagnosis of primary hyperoxaluria in patients with end-stage renal disease. *Nephron* 53: 81–82, 1989.
40. **Parks JH, Coe FL, Evan AP, Worcester EM.** Clinical and laboratory characteristics of calcium stone-formers with and without primary hyperparathyroidism. *BJU Int* 103: 670–678, 2008.
41. **Rouse D, Ng RC, Suki WN.** Calcium transport in the pars recta and thin descending limb of Henle of the rabbit perfused in vitro. *J Clin Invest* 65: 37–42, 1980.
42. **Salmond R, Seney FD.** Reset tubuloglomerular feedback permits and sustains glomerular hyperfunction after extensive renal ablation. *Am J Physiol Renal Fluid Electrolyte Physiol* 260: F395–F401, 1991.
43. **Scheid CR, Koul HK, Kennington L, Hill WA, Luber-Narod J, Jonassen J, Honeyman T, Menon M.** Oxalate-induced damage to renal tubular cells. *Scanning Microsc* 9: 1097–1105, 1995.
44. **Schwartz-Sorensen S, Amdisen A, Pedersen EBA.** Abnormal proximal tubular sodium handling in normotensive patients with chronic glomerulonephritis and normal glomerular filtration rate. *Scand J Clin Lab Invest* 47: 785–791, 1987.
45. **Shidham V, Chivukula M, Basir Z, Shidham G.** Evaluation of crystals in formalin-fixed, paraffin-embedded tissue sections for differential diagnosis of pseudogout, gout and tumoral calcinosis. *Mod Pathol* 14: 806–810, 2001.
46. **Sindic A, Chang MH, Mount DB, Romero MF.** Renal physiology of SLC26 anion exchangers. *Curr Opin Nephrol Hypertens* 16: 484–490, 2007.
47. **Sorensen SS, Amdisen A, Pedersen EB.** Abnormal proximal tubular sodium handling in normotensive patients with chronic glomerulonephritis and normal glomerular filtration rate. *Scand J Clin Invest* 47: 785–791, 1987.
48. **Stenvinkel P, Ottosson-Seeberger A, Alvestrand A.** Renal hemodynamics and sodium handling in moderate renal insufficiency: the role of insulin resistance and dyslipidemia. *J Am Soc Nephrol* 5: 1751–1760, 1995.
49. **Stokke ES, Ostensen J, Hartmann A, Kiii K.** Loop diuretics reduce lithium reabsorption without affecting bicarbonate and phosphate reabsorption. *Acta Physiol Scand* 140: 111–118, 1990.
50. **TietzeIN, Pedersen EB.** Renal haemodynamic changes, renal tubular function, sodium, and water homeostatic hormones in patients with chronic glomerulonephritis and in healthy humans after intravenous infusion of amino acids. *Nephrol Dial Transplant* 9: 499–504, 1994.
51. **Truong LD, Phung VT, Yoshikawa Y, Mattioli CA.** Glycoconjugates in normal human kidney. A histochemical study using 13 biotinylated lectins. *Histochemistry* 90: 51–60, 1988.
52. **Umekawa T, Byer K, Uemura H.** Diphenyleneiodium (DPI) reduces oxalate ion- and calcium oxalate monohydrate and brushite crystal-induced upregulation of MCP-1 in NRK 52E cells. *Nephrol Dial Transplant* 20: 870–878, 2005.
53. **Unwin RJ, Walter SJ, Shirley DG.** Lithium reabsorption in perfused loops of Henle: effects of perfusion rate and bumetanide. *Am J Physiol Renal Fluid Electrolyte Physiol* 266: F806–F812, 1994.
54. **Verhulst A, Asselman M, Naeyer SD, Vervaet BA, Mengel M, Gwinner W, D'Haese PC, Verkoelen CF, De Broe ME.** Preconditioning of the distal tubular epithelium of the human kidney precedes nephrocalcinosis. *Kidney Int* 68: 1643–1647, 2005.
55. **Vervaet BA, D'Haese PC, De Broe ME, Verhulst A.** Crystalluric and tubular epithelial parameters during the onset of intratubular nephrocalcinosis: illustration if the "fixed particle" theory in vivo. *Nephrol Dial Transplant* 24: 3659–3668, 2009.
56. **Vervaet BA, Verhuls TA, D'Haese PC, De Broe ME.** Nephrocalcinosis: new insights into mechanisms and consequences. *Nephrol Dial Transplant* 24: 2030–2035, 2009.
57. **Walter SJ, Shirley DG, Unwin RJ.** Effect of vasopressin on renal lithium reabsorption: a micropuncture and microperfusion study. *Am J Physiol Renal Fluid Electrolyte Physiol* 271: F223–F229, 1996.
58. **Wilson DM, Liedtke RR.** Modified enzyme-based colorimetric assay of urinary and plasma oxalate with improved sensitivity and no ascorbate interference: reference values and sample handling procedures. *Clin Chem* 37: 1229–1235, 1991.
59. **Worcester EM, Coe FL, Evan AP, Bergsland KJ, Parks JH, Willis LR, Clark DL, Gillen DL.** Evidence for increased postprandial distal nephron calcium delivery in hypercalciuric stone-forming patients. *Am J Physiol Renal Physiol* 295: F1286–F1294, 2008.
60. **Worcester Nakagawa Y EM, Bushinsky DA, Coe FL.** Evidence that serum calcium oxalate supersaturation is a consequence of oxalate retention in patients with chronic renal failure. *J Clin Invest* 77: 1888–1896, 1986.
61. **Zamlauski-Tucker MJ, Van Liew JB, Goldinger J, Noble B.** Persistent proximal tubule dysfunction late in Heymann nephritis. *Kidney Int* 37: 1536–1542, 1990.